Comparison of corrosion behavior of X65, 1Cr, 5Cr and 13Cr steels in water-containing supercritical CO_2 environments with SO_2/O_2

Yong Hua, Richard Barker, Georgios Bermperidis, Hongyuan Zhao and Anne Neville
Institute of Functional Surfaces
School of Mechanical Engineering
University of Leeds
Leeds, LS2 9JT
United Kingdom

Lei Zhang
Corrosion and Protection Centre
University of Science and Technology Beijing
30 Xueyuan Road
Beijing
China

ABSTRACT

A systematic study is presented to determine the corrosion behavior of four different steels (X65 carbon steel, 1Cr, 5Cr and 13Cr) that could be considered as pipeline/tubular materials for the transport and/or injection of supercritical CO_2 for carbon capture and storage (CCS) applications. The purpose of the research was to establish the influence of material selection on the critical water content required to avoid substantial levels of internal corrosion in an impure supercritical CO_2 system containing sulphur dioxide (SO_2) and oxygen (O_2). Experiments were performed in autoclaves containing supercritical CO_2 at 8 MPa and 35℃ in the presence of 100 ppm (mole) SO_2 with 20 or 1000 ppm O_2 under varying levels of humidity from 0 to 100%. General corrosion rates for all four materials were determined over a period of 48 hours via gravimetric analysis. Scanning electron microscopy (SEM), X-ray diffraction (XRD), and Raman spectroscopy were all implemented to assist in identifying surface corrosion products. Results from under-saturated experiments indicated that 13Cr steel enables a greater critical water content to be tolerated before corrosion occurs in the presence of 100 ppm SO_2 and 20/1000 ppm O_2. No corrosion attack was observed at a water content of 650 ppm for 13Cr, while X65, 1Cr and 5Cr produced general corrosion rates of ~0.01 mm/year. At water contents of 1200 ppm, corrosion rates for all materials remained below 0.05 mm/year in the presence of 100 ppm SO_2 and 20 ppm O_2, with 13Cr again exhibiting superior corrosion resistance. Increasing O_2 content to 1000 ppm had no significant effect on corrosion rates in under-saturated conditions. In water-saturated conditions at 100 ppm SO_2/20 ppm O_2 X65, 1Cr and 5Cr produced dramatically higher corrosion rates in the range of 0.7-0.8mm/year, whilst 13Cr maintained a low corrosion rate below 0.02 mm/year. Changing O_2 content to 1000 ppm in water-saturated conditions increased the corrosion rates of X65, 1Cr and 5Cr to ~0.9-1.1 mm/year and that of 13Cr to 0.65mm/year, indicating the material corrosion sensitivity to O_2 content. Comparison with previous results by the same authors indicated a noticeable synergy between SO_2 and O_2 which resulted in a greater degradation rate being observed compared to the sum of individual corrosion rates when SO_2 and O_2 were present independently at their respective concentrations in the water-saturated system. The research highlights that one option for controlling the corrosion rate under these specific impure supercritical CO_2 conditions may be through the implementation of 13Cr, although this may impose a significant cost penalty compared to carbon steels. The work shows that low Cr-bearing steels were unable to mitigate the effects of corrosion compared to X65 steel in these particular water-saturated conditions.

Key words: Supercritical CO_2, CO_2 corrosion, carbon steel, carbon capture and storage, sulfur dioxide, oxygen

INTRODUCTION

The transportation of dense phase CO_2 has been practiced for over 30 years with most pipelines being located in either the USA or Canada. According to literature, the majority of these pipelines transport CO_2 from natural sources, with a few carrying anthropogenic CO_2 from sites such as Canyon Reef Carriers[1, 2, 3, 4] and Weyburn[4, 5]. The CO_2 produced from natural sources is typically high purity, containing traces of impurities such as N_2, H_2O, CH_4 and H_2S. However, considering the impurities from anthropogenic sources, there is a significant difference in composition as the stream can become further contaminated by sulphur dioxide (SO_2), nitrogen oxides (NO_x), oxygen (O_2) and other components.

The various impurities within the CO_2 stream play an important role on transportation, influencing aspects such as health and safety considerations in the event of a release, process fluid operating regimes and pipeline corrosion management strategies. With regards to the transport and injection of CO_2, the most economically viable materials to construct pipelines from are carbon steel or low Cr-bearing steels (1-5Cr). However, carbon steels and low Cr steels are susceptible to corrosion from anthropogenic CO_2 when an aqueous phase forms within the system. Consequently, the water content is one of the most critical considerations when determining the propensity for corrosion to occur, as well as the extent of material degradation encountered. If the water content within the CO_2 stream locally exceeds the solubility limit, a separate aqueous phase will exist. If such a phase were to form on the pipeline wall it will invariably become saturated with CO_2, creating carbonic acid (H_2CO_3), lowering the pH of the aqueous phase and posing a threat to pipeline integrity[6, 7, 8]. Furthermore, the corrosion process can be accentuated by the additional presence of anthropogenic impurities such as SO_2, NO_x and O_2. There is a requirement to further understand the influence of such impurities on such corrosion processes to determine the critical water content for different pipeline materials in high pressure systems where supercritical CO_2 is the dominant phase.

The purpose of this work is to determine the susceptibility of API 5L (X65), 42CrMo4 (1Cr), X37CrMoV5-1 (5Cr) and X15Cr13 (13Cr) steels to water-containing supercritical CO_2 environments in the presence of SO_2 (100 ppm) and O_2 (20 and 1000 ppm) by measuring the general corrosion rates through the implementation of the weight loss method. A combination of scanning electron microscopy images (SEM), Raman spectra and XRD patterns are provided to indicate the morphological and compositional changes in the corrosion products produced in the presence of SO_2 and O_2.

EXPERIMENTAL PROCEDURES

Materials and preparation

Test specimens were machined from X65 carbon steel, 1Cr, 5Cr and 13Cr bars into discs with diameter of 25 mm and thickness of 6 mm. The chemical composition of all the steels is provided in Table 1. Surface preparation consisted of wet-grinding the entire sample up to 800 grit silicon carbide abrasive paper, rinsing with distilled water, followed by acetone, high purity ethanol and drying gently with compressed air. Samples were then stored in a desiccator until needed and weighed immediately before the experiment on an electronic balance with an accuracy of 0.001 mg before suspending inside the autoclave. Two samples were placed within the autoclave for each individual test.

A schematic representation of the experimental system layout has been shown in previous papers[9, 10]. The entire system consists of a 1 litre capacity autoclave, temperature controller, a $CO_2/SO_2/O_2$ mixed cylinder, a liquid CO_2 cylinder and a series of valves for CO_2 flow control.

All tests were conducted in static conditions in either water-saturated supercritical CO_2, or with the water content below the calculated solubility limit (under-saturated). According to Spycher et al.[11] the saturated water concentration in supercritical CO_2 at 35℃ and 8 MPa is 3437 ppm (mole). In order to ensure the water-saturated CO_2 condition, 34000 ppm of water was introduced to the bottom of the autoclave (not in direct contact with the sample) for the water-saturated tests (i.e. approximately 10 times the saturation limit).

Table 1: Elemental composition of X65, 1Cr, 5Cr and 13Cr steels evaluated in this study (wt.%)

	API 5L X65	42CrMo4 (1% Cr)	X37CrMoV5-1 (5% Cr)	X15Cr13 (13%Cr)
C	0.12	0.35-0.45	0.38	0.15
Si	0.18	0.1-0.35	1.00	1.00 max
Mn	1.27	0.5-0.8	0.4	1.00 max
P	0.008	0.035	-	0.04 max
S	0.002	0.05	-	0.035 max
Cr	0.11	0.9-1.5	5.00	11.5-13.5
Mo	0.17	0.2-0.4	1.30	-
Fe	Balance			

The entire matrix of the experimental conditions is provided in Table 2, which describes the different SO_2, O_2 and water contents that were evaluated. The distilled water used in this work was initially de-aerated by saturating the solution with CO_2 in a separate container for a minimum of 12 hours prior to testing. All the specimens were suspended within the autoclave on a non-conducting wire while also ensuring they were not in contact with the walls of the cylinder to prevent galvanic effects. The prepared, CO_2-saturated water was carefully delivered into the bottom of the autoclave at ambient pressure and temperature and sealed. All lines to the autoclave were then purged with CO_2 and evacuated to ensure the removal of initial traces of O_2 within the system. The required technical grade of CO_2/O_2/SO_2 mixture and liquid CO_2 was then transferred into the autoclave, heated and then pressurized to the correct temperature and pressure. The starting point of the test was taken from the time at which the autoclave reached the required temperature and pressure (35℃ and 8 MPa in this particul ar study).

At the end of each experiment the specimens were dried thoroughly and photographed. The samples were subsequently chemically cleaned to remove all traces of corrosion products before weighing. The cleaning process consisted of wiping the surface with a cotton pad soaked in Clarke's solution (20 g antimony trioxide + 50 g stannous chloride + 1000 ml hydrochloric acid) in accordance with ASTM[(1)] Standard G1-03[12]. This was followed by rinsing the samples with distilled water and then drying with compressed air.

The mass loss due to corrosion was determined from the weight difference before exposure and after cleaning. The corrosion rates were calculated by using Equation (1):

$$V_c = \frac{87600\Delta m}{\rho A t} \quad (1)$$

where V_c is the corrosion rate of the sample in mm/year, Δm is the weight loss in grams, ρ is the density of the sample in g/cm^3, A is the exposed area in cm^2 and t is the immersion time in hours.

Table 2: Test matrix for corrosion experiments

Temp (℃)	Pressure (Mpa)	Materials	H_2O (ppm)	SO_2 (ppm)	O_2 (ppm)	Immersion time (hours)
35	8	X65/1Cr/5Cr/13Cr	Above solubility limit of 3437 ppm through addition of 34000 ppm water	100	20 and 1000	48
			1200			
			650			
			300			

(1) ASTM International, 100 Barr Harbor Drive, West Conshohocken, PA 19428-2959.

RESULTS AND DISUSSIONS

X65, 1Cr, 5Cr and 13Cr steels exposed to water-containing supercritical CO_2 phase – 100 ppm SO_2 and 20 ppm O_2

Figure 1 shows the general corrosion rates (determined from mass loss measurements) of all four materials exposed to the water-containing supercritical CO_2 phase at 35℃ and 8 MPa, containing 100 ppm of SO_2 and 20 ppm of O_2. Figure 1(a) represents the experiments performed in under-saturated conditions, whilst Figure 1(b) shows that the corrosion rates obtained in water-saturated conditions. The corrosion rates in Figure 1(b) are supplemented with additional mass loss measurements for X65 recorded by the same authors in previous publications[13, 14, 15] to place the results into context. All samples were immersed in the test environment for a period of 48 hours in each experiment.

Figure 1(a) indicates that the general corrosion rates of all materials are below 0.01 mm/year when the water content is less than 650 ppm. No corrosion was recorded for any materials exposed to dry CO_2 i.e. with a water content of 0 ppm, as expected. Figure 1(a) also shows that as the water concentration increases, the general corrosion rates of each steel rise. For X65, 1Cr and 5Cr, an increase in water content from 300 to 650 ppm resulted in an increase in general corrosion rate from ~0.003 to ~0.006 mm/year. A further increase in water content to 1200 ppm produced general corrosion rates of ~0.008 to ~0.04 mm/year. No general corrosion was observed for 13Cr at water content of 650 ppm or below and this material exhibited the lowest general corrosion rate out of the four materials at a water content of 1200 ppm (0.003 mm/year). Figure 2 shows an SEM image of an X65 steel sample after 48 hours of immersion in the presence of 300 ppm water. This image is indicative of all other samples subjected to a water content of 300 ppm as well as 13Cr in the presence of 650 ppm. There was no visual indication of corrosion on any of these steel surfaces. SEM images of the samples after exposure to impure CO_2 containing 1200 ppm water are provided in Figure 3 and show minor indications of corrosion, corroborating with the low levels of mass loss from gravimetric analysis.

In all under-saturated experiments, the corrosion rate never exceeded 0.05 mm/year for all four materials at water contents up to 1200 ppm. However, experiments performed in the water-saturated phase produced more substantial rates of corrosion. As shown in Figure 1(b) the general corrosion rates of X65, 1Cr, 5Cr and 13Cr reached 0.72, 0.79, 0.79 and 0.01 mm/year, respectively in the presence of water-saturated CO_2 containing 100 ppm SO_2 and 20 ppm O_2. The effect of the presence of the SO_2/O_2 mixture becomes distinctly more noticeable as the water content in the system rises, with the exception of 13Cr which exhibited a significantly lower corrosion rate of 0.01 mm/year. To put these corrosion rates into context, Figure 1(b) also provides the general corrosion rate from a previous publication[14] for X65 steel under the same operating temperature and pressure. These experiments were performed in the absence of both SO_2 and O_2, but also with 20 ppm O_2 and 100 ppm SO_2 presence separately in the water-saturated CO_2 phase. The low corrosion rate of 0.1 mm/year observed in the absence of SO_2 and O_2 (0.1 mm/year) demonstrates the significant role the combination of these impurities can play in accelerating the corrosion process. The combined addition of SO_2 and O_2 resulted in a 7-fold increase in the rate of materials dissolution compared to the system with only water as the impurity. However, considering the corrosion rates recorded when only 100 ppm SO_2 and 20 ppm O_2 are present (0.7 and 0.09 mm/year, respectively) it appears that the dramatic increase in corrosion is predominantly attributed to the presence of SO_2, at least in the case of X65 steel. The most interesting observation is that the addition of 20 ppm O_2 alone to the water-saturated system reduced the general corrosion rates from the system without SO_2 and O_2 (0.1 down to 0.09 mm/year) whilst the addition of 20 ppm O_2 to the system containing 100 ppm SO_2 increased corrosion rate (0.69 to 0.72 mm/year). This observation indicates there may be a potential synergistic effect between both SO_2 and O_2 which can lead to higher degradation rates when the two species are co-present compared to the rates of their individual effects added together in separate experiments. Unfortunately, the difference is not significant enough to reach this conclusion from these particular experiments.

Figure 4 shows the scanning electron microscopy images of X65, 1Cr, 5Cr and 13Cr exposed to water-containing supercritical CO_2 condition in the presence of 100 ppm SO_2 and 20 ppm O_2. The images indicate a significant increase in the extent of corrosion for X65, 1Cr and 5Cr whilst 13Cr only exhibited small regions where corrosion products could be identified. The nature of the corrosion products is considered in detail in a subsequent section and related to the synergistic effect observed between both O_2 and SO_2.

X65, 1Cr, 5Cr and 13Cr steels exposed to water-containing supercritical CO_2 phase – 100 ppm SO_2 and 1000 ppm O_2 (Effect of increasing O_2 content)

Figure 5 shows the general corrosion rates of all materials in water-containing supercritical CO_2 environments at 35℃ and 8 MPa. Figure 5(a) indicates that for under-saturated conditions, the increase in O_2 content from 20 to 1000 ppm resulted in no dramatic change in the uniform degradation rates recorded, with all general corrosion rates being below 0.03 mm/year at water contents of 1200 ppm and under. No corrosion was observed for 5Cr at a water content of 300 ppm or for 13Cr at 650 ppm water and below.

Figure 5(b) provides the general corrosion rates recorded for X65, 1Cr, 5Cr and 13Cr exposed to water-saturated conditions in the combined presence of 100 ppm SO_2/1000 ppm O_2. The results are supplemented with previously performed experiments in the absence of O_2 and SO_2, along with tests where 1000 ppm O_2 and 100 ppm SO_2 were evaluated separately.

Considering the tests containing 100 ppm SO_2 and 1000 ppm O_2 in Figure 5(b) (blue charts), the general corrosion rates were recorded at 0.95, 1.00, 1.10 and 0.65 mm/year for X65, 1Cr, 5Cr and 13Cr, respectively. The increase in O_2 level from 20 to 1000 ppm clearly plays an important role in influencing the general corrosion rates in water-saturated conditions when present with SO_2, increasing corrosion rates from ~0.7 – 0.8 mm/year at 20 ppm in Figure 1(b) to ~0.95 – 1.10 in Figure 5(b) mm/year for X65, 1Cr and 5Cr. Although it is apparent that 13Cr has superior general corrosion resistance in the supercritical CO_2 environment in the presence of 100 ppm SO_2 with 20/1000 ppm O_2 compared to the other three materials (X65, 1Cr and 5Cr), 13Cr is still significantly affected by the increase in O_2 in water-saturated conditions. The increase in O_2 content increased the general corrosion of 13Cr from 0.01 to 0.65 mm/year.

Reflecting on previous experiments for X65 (red charts in Figure 5(b)) in comparison to this work, the observations are similar to those in Figure 1(b) in that 1000 ppm O_2 alone reduces general corrosion rates from that of the system containing only water and CO_2 (0.1 to 0.03 mm/year). The ability of O_2 to reduce the general corrosion of carbon steel in a CO_2 environment is not a new observation and has been reported by other authors[16]. This observation is potentially attributed to the passivating effect of iron oxide species on the steel surface in such environments, but this remains to be confirmed in this particular study. What is clear is that O_2 has no detrimental effect on general corrosion in a CO_2-H_2O-O_2 system up to a concentration of 1000 ppm under these particular conditions for carbon steel. However, when 1000 ppm O_2 is introduced to the system containing 100 ppm SO_2 a distinct synergy is observed, corroborating with the potential synergy initially suggested in Figure 1(b) at lower O_2 contents. However, under these conditions the synergy is much more distinct. The addition of 1000 ppm O_2 to the system containing SO_2 resulted in general corrosion increasing from 0.7 to 0.95 mm/year, producing a noticeable synergistic effect.

Figure 6 presents a representative scanning electron microscope (SEM) image for all four steels exposed to under-saturated supercritical CO_2 conditions in the presence of 100 ppm SO_2 and 1000 ppm O_2 with 300 ppm water. No measureable corrosion was recorded until a water content of 650 ppm and 1200 ppm were reached for 5Cr and 13Cr, respectively. SEM images in Figure 7 for a water content of 1200 ppm corroborate with the mass loss measurements in that small amounts of corrosion are observed on the four materials. Figure 8 indicated that in the water-saturated environment, a significant level of corrosion has occurred, producing a cracked corrosion product film with a similar morphology on all of the steel sample surfaces.

In terms of the comparison of the different materials in this study, Choi et al.[17] also compared the corrosion behavior of X65 steel with that of 13Cr in impure supercritical CO_2. They found that in water-saturated CO_2 at 50℃ and 8 MPa with 0.33 MPa O_2 and 0.08 MPa SO_2, there was no difference in corrosion rates between the two materials, with both steels producing rates of dissolution equivalent to ~7mm/year. The general corrosion rates in this study of 0.95 and 0.65 mm/year for X65 and 13Cr reflect a much lower level of material dissolution which can be attributed to the reduced level of impurities. Under these particular conditions the results demonstrate that 13Cr does offer superior corrosion protection to both X65 and low Cr steels, however, increasing O_2 content in the system reduces 13Cr performance substantially. The low Cr-bearing steels did not offer improved corrosion resistance compared to X65 in the water-saturated environment.

The influence of SO_2 and O_2 on corrosion product formation

To identify the nature of corrosion products on the steel surface, XRD and Raman spectroscopy were employed and the resulting patterns and spectra as shown in Figures 9 and 10, respectively. Raman spectroscopy was used in conjunction with XRD on X65 samples to detect the presence of any potentially amorphous products, as well as to provide a localized form of corrosion product analysis.

The XRD patterns for the samples exposed to the water-saturated environments containing 100 ppm SO_2 and 20 ppm/1000 ppm O_2 are provided in Figure 9. In the system containing 100 ppm SO_2 and 20 ppm O_2, the presence of $FeSO_3 \cdot 3H_2O$ and $FeCO_3$ were detected using XRD measurements for X65, 1Cr and 5Cr.

An increase in O_2 content to 1000 ppm still resulted in $FeSO_3 \cdot 3H_2O$ and $FeCO_3$ being detected by XRD measurements (Figure 9) for X65 and 1Cr. It is interesting to note that no $FeSO_3 \cdot 3H_2O$ crystals were detected by XRD for 5Cr and 13Cr (however, the use of localized Raman spectroscopy produced peaks at 960 cm^{-1}, 974 cm^{-1} and 990 cm^{-1} confirming that both $FeSO_3 \cdot 3H_2O$ and $FeSO_4.xH_2O$ were also present on the steel surface).

To evaluate the corrosion behaviour of the X65 steel more closely in an attempt to explain the synergistic effect between O_2 and SO_2, localized Raman spectroscopy was employed. Typical spectra are provided in Figures 10(a) and (b) for experiments at 20 ppm and 1000 ppm O_2 respectively. Again, both $FeCO_3$ and $FeSO_3$ were detected. The strongest peak on the Raman spectra observed at 1085 cm^{-1} in Figure 10(a) is representative of $FeCO_3$. The strongest Raman peak at 960 cm^{-1} relates to $FeSO_3$ and the vibrational wavenumbers between ~3200 and 3400 cm^{-1} are related to the degree of hydration.

Although no $FeSO_4$ was found on any of the steels surfaces in the presence of 100 ppm SO_2 and 20 ppm O_2 using XRD, a small peak at ~985-990 cm^{-1} in Figure 10(a) on the Raman spectra suggests that $FeSO_4$ may also exist on the surface. The detection of $FeSO_4$ on X65 was more substantial at 1000 ppm O_2, suggesting that the synergistic effect relating to the increase in corrosion rate manifests itself through the formation of greater quantities of H_2SO_4 which results in precipitation of $FeSO_4$ on the steel surface.

In terms of the role of O_2 and SO_2 on the observed synergistic effect, some significant reactions mechanisms have been suggested by both Choi et al.,[17], Farelas et al.,[18] and Xiang et al.,[19, 20]. Firstly, SO_2 is believed to dissolve into the condensed water film on the surface and subsequently becomes ionized:

$$H_2O + SO_2 \rightarrow H^+ + HSO_3^{2-} \quad (2)$$

$$HSO_3^{2-} \rightarrow H^+ + SO_3^{2-} \quad (3)$$

The cathodic reaction is then permitted through the direct reduction of hydrogen ions:

$$2\mathrm{H}^+ + 2\mathrm{e}^- \leftrightarrow \mathrm{H}_2 \quad (4)$$

In the presence of O_2, sulphite ions are capable for being oxidised to sulphate ions:

$$SO_3^{2-} + \frac{1}{2}O_2 \rightarrow SO_4^{2-} \quad (5)$$

$FeCO_3$, $FeSO_3$ and $FeSO_4$ then form via their respective precipitation processes:

$$Fe^{2+} + CO_3^{2-} \rightarrow FeCO_3 \quad (6)$$

$$Fe^{2+} + SO_3^{2-} \rightarrow FeSO_3 \quad (7)$$

$$Fe^{2+} + SO_4^{2-} \rightarrow FeSO_4 \quad (8)$$

Choi et al.[17] also suggested that if the O_2 concentration is enough in such systems that $FeSO_4$ can undergo further oxidation to become FeOOH in an acid regeneration process, although this cannot be confirmed in this study:

$$4\mathrm{Fe}SO_4 + 6H_2O + O_2 \rightarrow 4FeOOH + 4H_2SO_4 \quad (9)$$

As mentioned, the detection of $FeSO_3$ and $FeSO_4$ are consistent with observations by Choi et al.,[17] whose experiments were performed in the presence of much higher O_2 and SO_2 contents. In their tests, $FeSO_4$ was reported to have formed on X65 in the presence of 1% (0.08 MPa) SO_2 with O_2. The results presented here show that the lower SO_2 and O_2 content (100 ppm and 1000 ppm respectively) still resulted in trace amounts of $FeSO_4$. As O_2 content was increased to 1000 ppm, the oxidation of all sulphite ions to sulphate ions became more significant, resulting in detectable quantities of $FeSO_4$ on the X65 steel surface through Raman spectroscopy and a noticeable synergy between the two species resulting in the enhancement of the rate of material dissolution.

CONCLUSIONS

The research presented has focused towards quantifying the extent of the general corrosion of X65 carbon steel, 1Cr, 5Cr and 13Cr steels in water-containing supercritical CO_2 environments containing 100 ppm SO_2 with 20 ppm and 1000 ppm of O_2, representative of dense phase anthropogenic CO_2 transport. Tests were conducted at a pressure of 8 MPa and a temperature of 35℃ for 48 hours in an effort to understand diff erent material performance, but also to understand the potential synergistic effect between SO_2 and O_2. From out study the following conclusions can be made:

- In conditions containing 100 ppm SO_2 and 20 ppm O_2, general corrosion rates of all materials was below 0.05 mm/year when the dissolved water content was 1200 ppm and below.
- Increasing O_2 content to 1000 ppm in the presence of 100 ppm SO_2 had no significant effect on general corrosion rates for the four materials in under-saturated conditions.
- In water-saturated conditions containing 100 ppm SO_2 and 20 ppm O_2, 1Cr and 5Cr exhibited no improvement on corrosion resistance compared to X65, with corrosion rates ranging between 0.7 and 0.8 mm/year. However, 13Cr showed superior corrosion resistance with a corrosion rate of 0.02 mm/year.
- Increasing O_2 content to 1000 ppm O_2 in the presence of 100 ppm SO_2 increased general corrosion rates from the 100 ppm SO_2/20 ppm O_2 system to 0.9-1.1 mm/year for X65, 1Cr and 5Cr. However, the most significant increase in corrosion rate was observed for 13Cr where general corrosion increased from 0.02 to 0.65 mm/year.
- Comparison of general corrosion rates with previous results by the same authors indicated a noticeable synergy between SO_2 and O_2 which resulted in a greater degradation rate being observed compared to the sum of individual corrosion rates when SO_2 and O_2 are present independently at their respective concentrations in the water-saturated system. Localised Raman spectra of the X65 corrosion products revealed the presence of $FeSO_3$, $FeCO_3$ and $FeSO_4$. The extent of $FeSO_4$ detected using Raman spectroscopy increased with higher O_2 content, suggesting that the synergistic effect relating to the increase in corrosion rate manifests itself through the formation of greater quantities of H_2SO_4 (through the oxidation of sulphite ions to sulphate ions) resulting in precipitation of $FeSO_4$ on the steel surface.

ACKNOWLEDGEMENTS

Dr Barker would like to express his thanks to the National Association of Corrosion Engineers (NACE) and their technical committee for their financial support which provided him and his research colleagues with the opportunity to contribute towards the research area of corrosion in CO2 transportation pipelines and also enabled them to write this paper.

REFERENCES

1. F.W. Schremp and R.G. Roberson, "Effect of Supercritical Carbon Dioxide (CO_2) on Construction Materials".
2. A. Oosterkamp and J. Ramsen, State-of-the-art overview of CO_2 pipeline transport with relevance to offshore pipelines. Polytech Report No: POL-O-2007-138-A, 2008.
3. J. Gale and J. Davison, Transmission of CO_2—safety and economic considerations. Energy, 2004. 29(9–10): p. 1319-1328.
4. M.E. Boot-Handford, J.C. Abanades, E.J. Anthony, M.J. Blunt, S. Brandani, N. Mac Dowell, J.R. Fernandez, M.-C. Ferrari, R. Gross, J.P. Hallett, R.S. Haszeldine, P. Heptonstall, A. Lyngfelt, Z. Makuch, E. Mangano, R.T.J. Porter, M. Pourkashanian, G.T. Rochelle, N. Shah, J.G. Yao, and P.S. Fennell, Carbon capture and storage update. Energy & Environmental Science, 2014. 7(1): p. 130-189.
5. E.D. Visser, C. Hendriks, M. Barrio, M.J. Mølnvik, G.D. Koeijer, S. Liljemark, and Y.L. Gallo, Dynamis CO_2 quality recommendations. International Journal of Greenhouse Gas Control, 2008. 2(4): p. 478-484.
6. I.S. Cole, D.A. Paterson, P. Corrigan, S. Sim, and N. Birbilis, State of the aqueous phase in liquid and supercritical CO_2 as relevant to CCS pipelines. International Journal of Greenhouse Gas Control, 2012. 7(0): p. 82-88.
7. F. Pessu, R. Barker, and A. Neville. The Influence of pH on Localized Corrosion Behavior of X65 (UNS K03014) Carbon Steel in CO_2-Saturated Brines. in CORROSION 2015. 2015: NACE International.
8. Y. Hua, R. Barker, and A. Neville, Comparison of corrosion behaviour for X-65 carbon steel in supercritical CO_2-saturated water and water-saturated/unsaturated supercritical CO_2 The Journal of Supercritical Fluids, 2015. 97: p. 224-237.
9. Y. Hua, R. Barker, and A. Neville, Effect of temperautre on the critical water content for general and localised corrosion of X65 carbon steel in the transport of supercritical CO_2. The International Journal of Greenhouse Gas Control, 2014. 31: p. 48-60.
10. Y. Hua, R. Barker, C. T, M. Ward, and A. Neville, Relating Iron Carbonate Morphology to Corrosion Characteristics for Water-Saturated Supercritical CO_2 Systems. The Journal of Supercritical Fluids, 2014. vol. 98: p. 183-193.
11. N. Spycher, K. Pruess, and J. Ennis-King, CO_2-H_2O mixtures in the geological sequestration of CO_2. I. Assessment and calculation of mutual solubilities from 12 to 100℃ and up to 600 b ar. Geochimica et Cosmochimica Acta, 2003. 67(16): p. 3015-3031.
12. ASTM. Standard G1-03, Standard practice for preparing, cleaning, and evaluating corrosion test specimens. ASTM International: West Conshohocken, PA, 2003.
13. Y. Hua, R. Barker, and A. Neville, Understanding the Influence of SO_2 and O_2 on the Corrosion of Carbon Steel in Water-Saturated Supercritical CO_2. Corrosion, 2014: p. Article In Press.
14. Y. Hua, R. Barker, and A. Neville, The influence of SO_2 on the tolerable water content to avoid pipeline corrosion during the transportation of supercritical CO_2. International Journal of Greenhouse Gas Control, 2015. 37: p. 412-423.
15. Y. Hua, R. Barker, and A. Neville, The effect of O_2 content on the corrosion behaviour of X65 and 5Cr in water-containing supercritical CO_2 environments. Applied Surface Science, 2015. 356: p. 499-511.
16. G. Schmitt, and M. Horstemeier. Fundamental aspects of CO_2 metal loss corrosion-Part II: Influence of different parameters on CO_2 corrosion mechanisms. in CORROSION 2006. 2006: NACE International.
17. Y.-S. Choi, S. Nešić, and D. Young, Effect of impurities on the corrosion behavior of CO_2 transmission pipeline steel in supercritical CO_2−water environments. Environmental Science & Technology, 2010. 44(23): p. 9233-9238.
18. F. Farelas, Y.-S. Choi, and S. Nesic, "Effects of CO_2 phase change, SO_2 content and flow on the corrosion of CO_2 transmission pipeline steel", in CORROSION 2012. 2012: Salt Lake City, UT:NACE.
19. Y. Xiang, Z. Wang, X.X. Yang, Z. Li, and W.D. Ni, The upper limit of moisture content for supercritical CO_2 pipeline transport. The Journal of Supercritical Fluids, 2012. 67: p. 14-21.
20. Y. Xiang, Z. Wang, C. Xu, C.C. Zhou, Z. Li, and W.D. Ni, Impact of SO_2 concentration on the corrosion rate of X70 steel and iron in water-saturated supercritical CO_2 mixed with SO_2. The Journal of Supercritical Fluids, 2011. 58(2): p. 286-294.

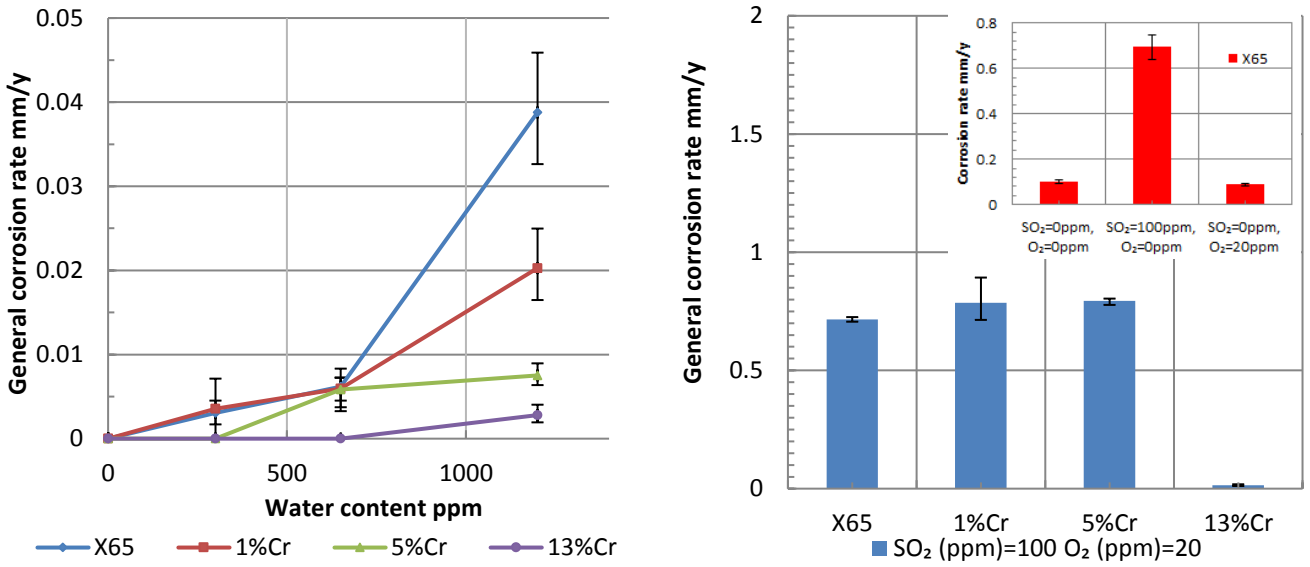

Figure 1: Corrosion rates of X65/1Cr/5Cr/13Cr samples in water-containing supercritical CO_2 phase at 8 MPa **and 35℃ over an exposure time of 48 hours (a) under-saturated, (b) water-saturated conditions in the presence of 100 ppm SO_2 and 20 ppm O_2.**

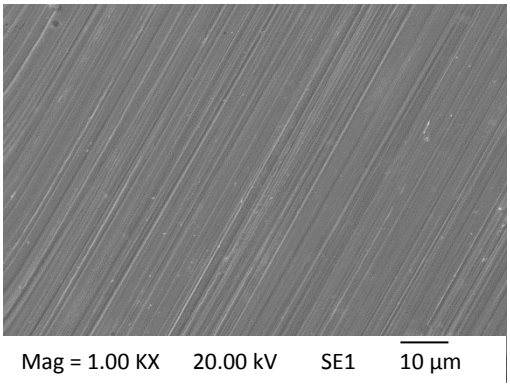

Figure 2: SEM image of X65 sample exposed to under-saturated dense phase CO_2 with 100 ppm SO_2, 20 ppm O_2 and water content of 300 ppm; image is also indicative of 1Cr/5Cr/13Cr at 300 ppm water and 13Cr at 650 ppm in that no corrosion was observed on any sample after 48 h

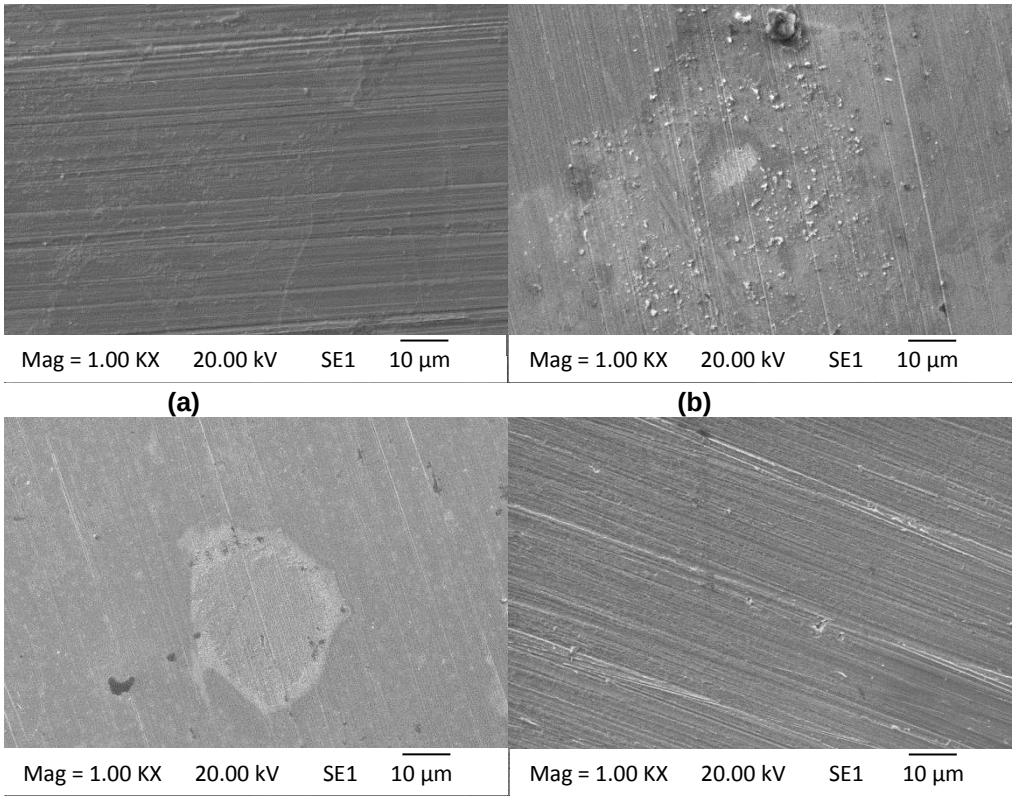

Figure 3: SEM images of (a) X65, (b) 1Cr, (c) 5Cr and (d) 13Cr samples exposed to under-saturated dense phase CO_2 with 100 ppm SO_2, 20 ppm O_2 and water content of 1200 ppm after 48 h

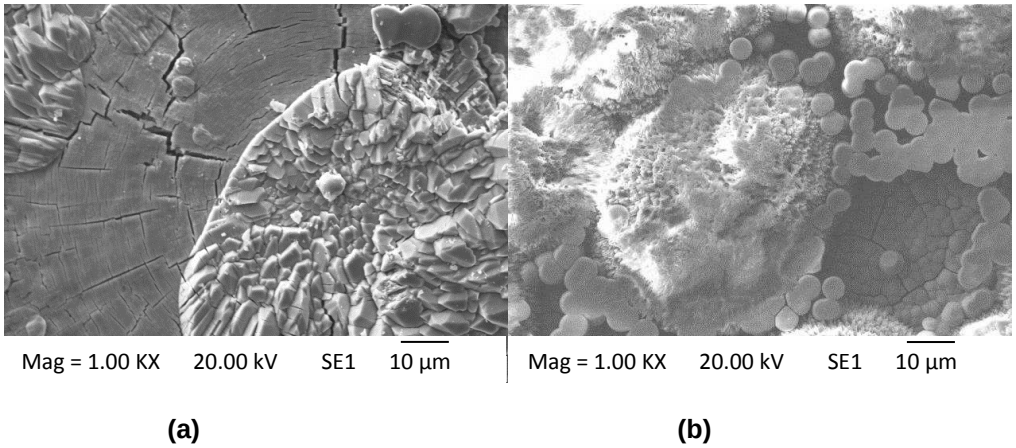

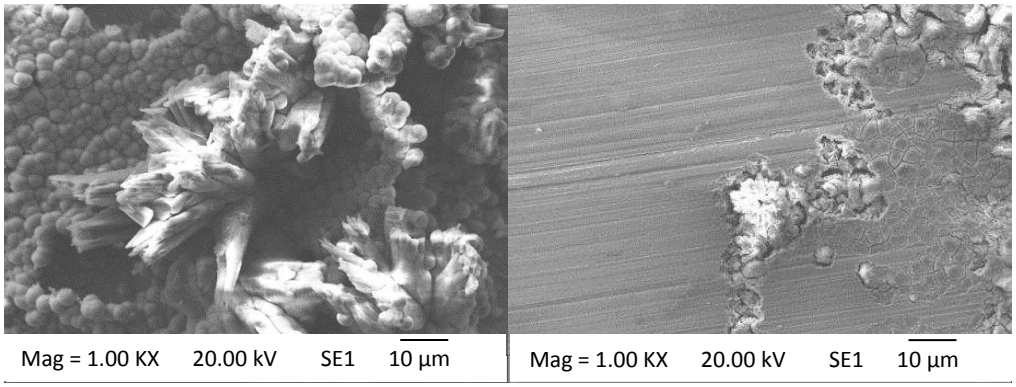

(c) (d)

Figure 4: SEM images of (a) X65, (b) 1Cr, (c) 5Cr and (d) 13Cr samples exposed to water-saturated dense phase CO_2 with 100 ppm SO_2, 20 ppm O_2 after 48 h

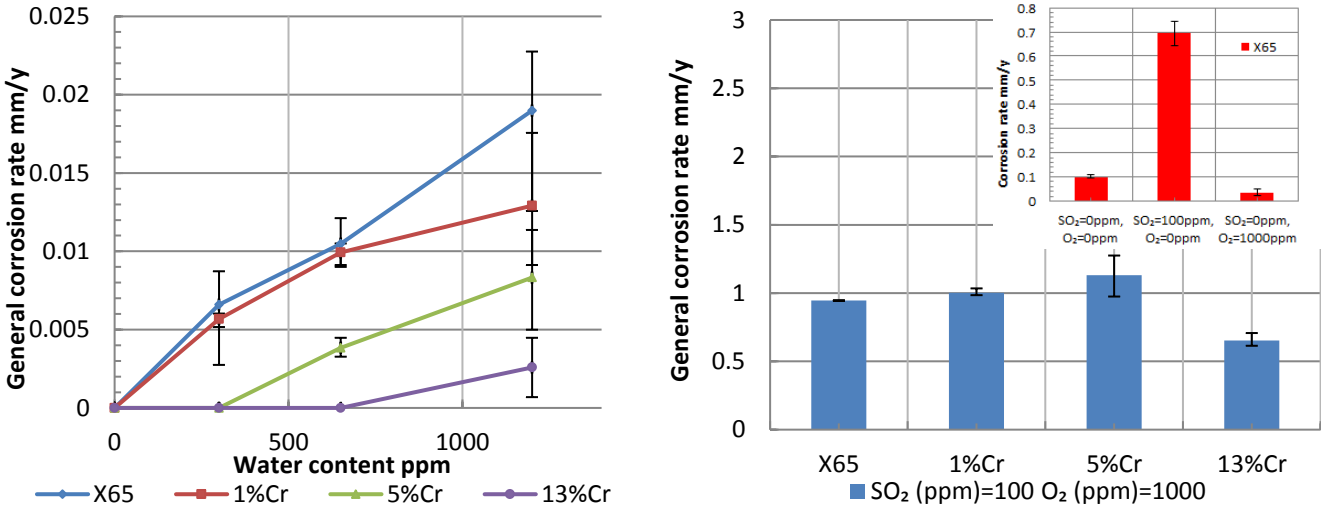

(a) (b)

Figure 5: Corrosion rates of X65/1Cr/5Cr/13Cr samples in water-containing supercritical CO_2 phase at 8 MPa **and 35℃ over an exposure time of 48 hours (a) under-saturated, (b) water-saturated conditions in the presence of 100 ppm SO_2 and 1000 ppm O_2.**

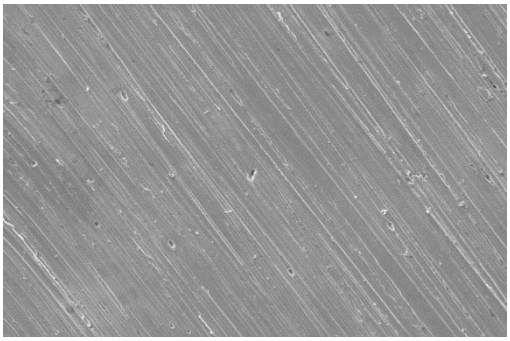

Figure 6: SEM image of X65 sample exposed to under-saturated dense phase CO_2 with 100 ppm SO_2, 1000 ppm O_2 and water content of 300 ppm; image is also indicative of 1Cr/5Cr/13Cr at 300 ppm water and 13Cr at 650 ppm in that no corrosion was observed on any sample after 48 h

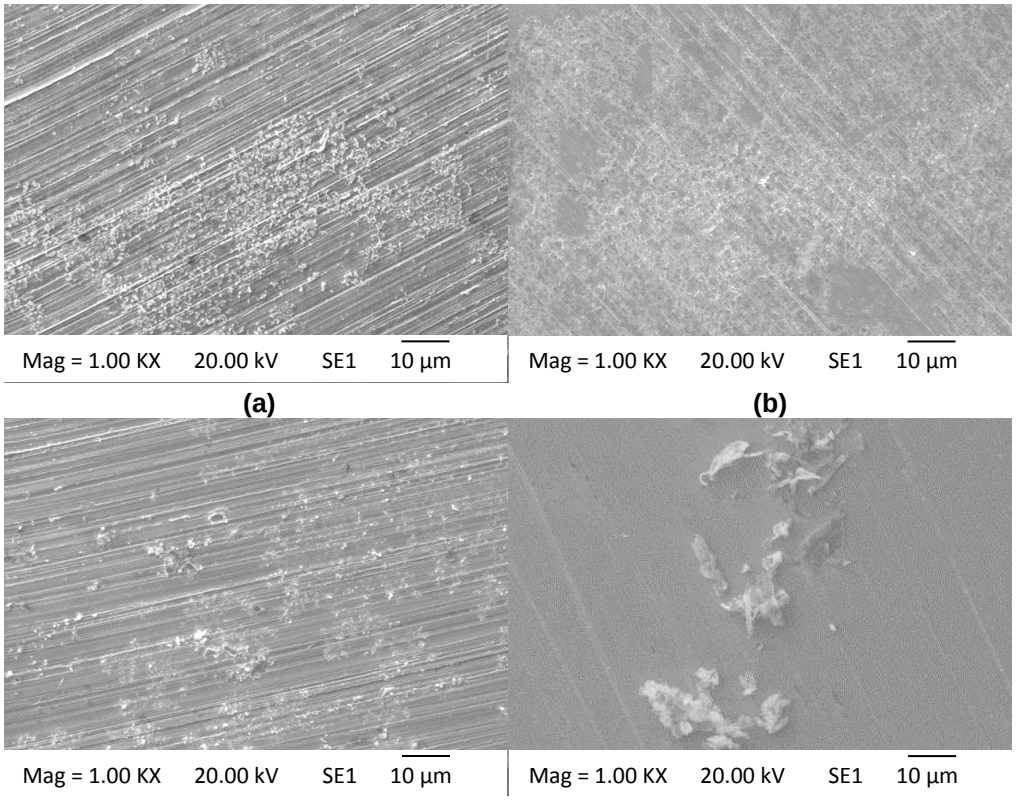

Figure 7: SEM images of (a) X65, (b) 1Cr, (c) 5Cr and (d) 13Cr samples exposed to under-saturated dense phase CO_2 with 100 ppm SO_2, 1000 ppm O_2 and water content of 1200 ppm after 48 h

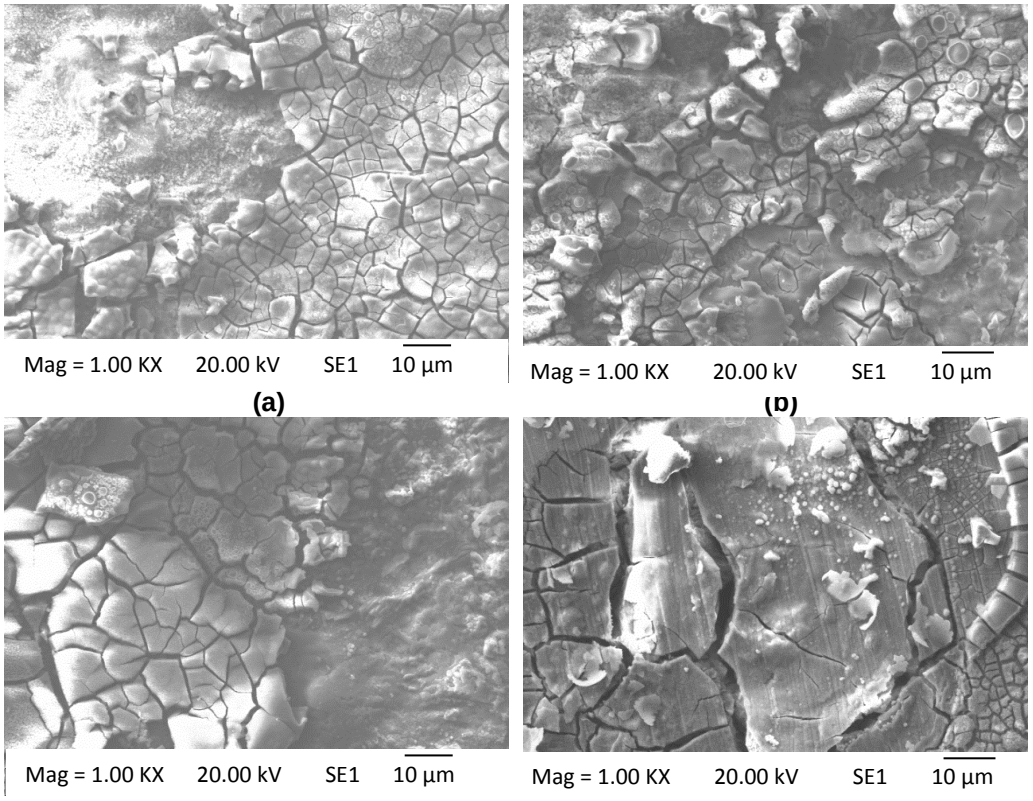

Figure 8: SEM images of (a) X65, (b) 1Cr, (c) 5Cr and (d) 13Cr samples exposed to water-saturated dense phase CO_2 with 100 ppm SO_2, 1000 ppm O_2 after 48 h

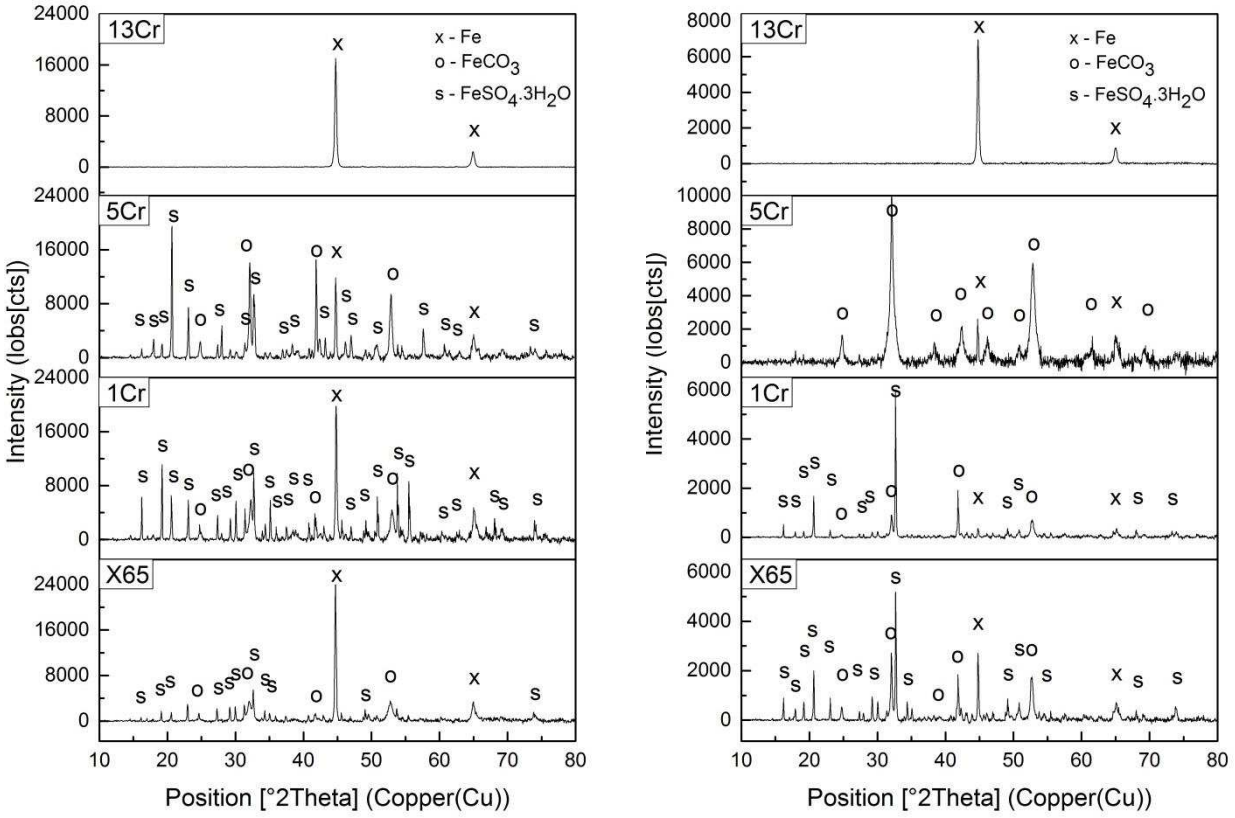

(a) **(b)**

Figure 9: XRD pattern of X65, 1Cr, 5Cr and 13Cr samples exposed to water-saturated dense phase CO_2 containing 100 ppm SO_2 with 20 ppm (a) or 1000 ppm (b) O_2 at 35℃ and 8 MPa **after 48 hours**

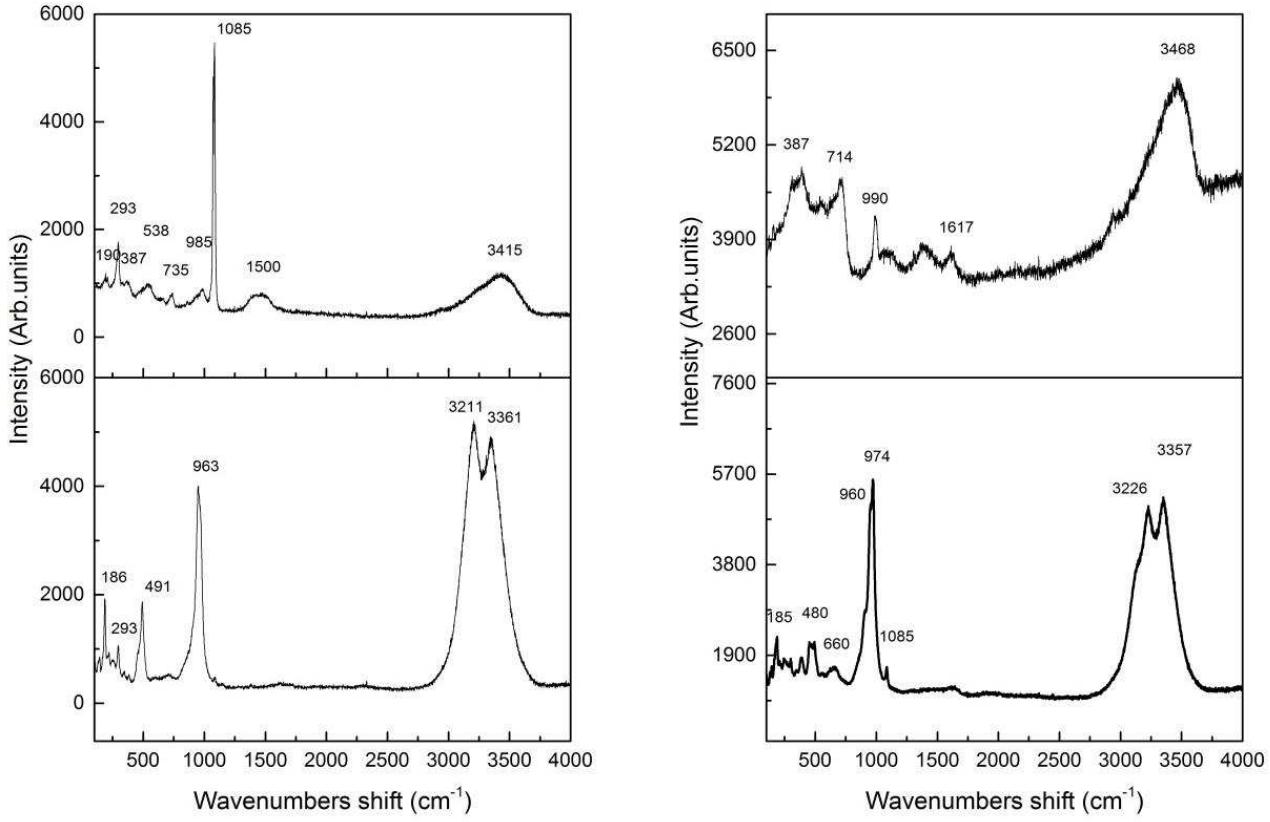

(a) **(b)**

Figure 10: Example of Raman spectra of X65 sample exposed to water-saturated supercritical CO_2 phase at 35℃ and 8 MPa **containing (a) 100 ppm SO_2 and 20 ppm O_2 and (b) 100 ppm SO_2 and 1000 ppm O_2.**